Characterization of a Transient Intermediate Formed in the Liver Alcohol Dehydrogenase Catalyzed Reduction of 3-Hydroxy-4-nitrobenzaldehyde†

Alastair K. H. MacGibbon,‡ Steven C. Koerber,§ Kathleen Pease, and Michael F. Dunn*
Department of Biochemistry, University of California, Riverside, Riverside, California 92521-0129
Received August 26, 1986; Revised Manuscript Received December 19, 1986

ABSTRACT: The compounds 3-hydroxy-4-nitrobenzaldehyde and 3-hydroxy-4-nitrobenzyl alcohol are introduced as new chromophoric substrates for probing the catalytic mechanism of horse liver alcohol dehydrogenase (LADH). Ionization of the phenolic hydroxyl group shifts the spectrum of the aldehyde from 360 to 433 nm (pK_a = 6.0), whereas the spectrum of the alcohol shifts from 350 to 417 nm (pK_a = 6.9). Rapid-scanning, stopped-flow (RSSF) studies at alkaline pH show that the LADH-catalyzed interconversion of these compounds occurs via the formation of an enzyme-bound intermediate with a blue-shifted spectrum. When reaction is limited to a single turnover of enzyme sites, the formation and decay of the intermediate when aldehyde reacts with enzyme-bound reduced nicotinamide adenine dinucleotide E(NADH) are characterized by two relaxations ($\lambda_f \simeq 3\lambda_s$). Detailed stopped-flow kinetic studies were carried out to investigate the disappearance of aldehyde and NADH, the formation and decay of the intermediate, the displacement of Auramine O by substrate, and ^2H kinetic isotope effects. It was found that (1) NADH oxidation takes place at the rate of the slower relaxation (λ_s); (2) when NADD is substituted for NADH, λ_s is subject to a small primary isotope effect (λ_s^H/λ_s^D = 2.0); and (3) the events that occur in λ_s precede λ_f. These findings identify the intermediate as a ternary complex containing bound oxidized nicotinamide adenine dinucleotide (NAD^+) and some form of 3-hydroxy-4-nitrobenzyl alcohol. The blue-shifted spectrum of the intermediate strongly implies a structure wherein the phenolic hydroxyl is neutral. When constrained to a mechanism that assumes only the neutral phenolic form of the substrate binds and reacts and that the intermediate is an E(NAD^+, product) complex, computer simulations yield RSSF and single-wavelength time courses that are qualitatively and semiquantitatively consistent with the experimental data. We conclude that the LADH substrate site can be divided into two subsites: a highly polar, electropositive subsite in the vicinity of the active-site zinc and, just a few angstroms away, a rather nonpolar region. The polar subsite promotes formation of the two interconverting reactive ternary complexes. The nonpolar region is the binding site for the hydrocarbon-like side chains of substrates and in the case of 3-hydroxy-4-nitrobenzaldehyde conveys specificity for the neutral form of the phenolic group.

A variety of chromophoric substrates, substrate analogues, and/or chromophoric enzyme derivatives have been used to investigate the physicochemical events that occur during liver alcohol dehydrogense (LADH)[1] catalysis. These studies have resulted in the discovery of at least three types of chemical intermediates along the reaction path. The investigation of the properties of these intermediates has substantially added to our understanding of the roles played by the active-site zinc, the coenzyme, and protein conformational changes during catalysis (Bernhard et al., 1970; Dunn & Hutchison, 1973; Dunn, 1974; Koerber et al., 1980, 1983; Dunn et al., 1982, 1986; Cedergren-Zeppezauer et al., 1982; Gerber et al., 1983; Dahl & Dunn, 1984a,b; Abdallah et al., 1984; Sartorius et al., 1987). These studies have established that (1) aldehyde reduction occurs via inner-sphere coordination of the aldehyde carbonyl to the active-site zinc ion; (2) NADH plays a noncovalent effector role in the formation of this activated intermediate (Dunn & Hutchison, 1973; Dunn et al., 1982; Cedergren-Zeppezauer et al., 1982); (3) during aldehyde reduction, hydride transfer precedes proton transfer (Morris et al., 1980); (4) conversely, coordinated alkoxide ion is the *reactive* species that undergoes oxidation (Dunn, 1974; Kvassman et al., 1981; Koerber et al., 1983; Gerber et al., 1983; Dunn et al., 1986; Sartorius et al., 1987); and (5) there are two inner-sphere-coordinated alcohol ternary complexes along the reaction path, and the interconversion of these two intermediates appears to be linked to an enzyme isomerization (Gerber et al., 1983; Sartorius et al., 1987).

The chromophoric substrate *trans*-4-(*N*,*N*-dimethylamino)cinnamaldehyde (DACA)[1] has been found to be a sensitive indicator of the nature and strength of the microscopic electrostatic force fields at the LADH catalytic site (Dunn & Hutchison, 1973; Dunn et al., 1982, 1986; Dahl & Dunn, 1984a,b; Sartorius et al., 1987). When it is bound to the LADH active site in ternary complexes with NADH and NAD^+, the long-wavelength π,π^* transition of the DACA chromophore is highly perturbed. These perturbations are the result of the summed electrostatic field contributions of the

† This work was supported by National Science Foundation Grants PCM 7911526, PCM 8108862, and DMB 8408513.
* Address correspondence to this author.
‡ Present address: Dairy Research Institute, Palmerston North, New Zealand.
§ Present address: Department of Biochemistry and Biophysics, School of Medicine, University of California, San Francisco, San Francisco, CA 94143, and Molecular Biology Division, Veterans Administration Medical Center, San Francisco, CA 94121.

[1] Abbreviations: LADH or E, horse liver alcohol dehydrogenase (EC 1.1.1.1); S and P, substrate and product, respectively; NAD^+ and NADH, oxidized and reduced nicotinamide adenine dinucleotide, respectively; NADD, (4*R*)-4-deuterio-NADH; DACA, *trans*-4-(*N*,*N*-dimethylamino)cinnamaldehyde; Pyr, pyrazole; HOnPhCHO and $^-$OnPhCHO, the neutral and ionized forms, respectively, of 3-hydroxy-4-nitrobenzaldehyde; $HOnPhCH_2OH$ and $^-OnPhCH_2OH$, the neutral and ionized forms, respectively, of the 3-hydroxyl group of 3-hydroxy-4-nitrobenzyl alcohol; $HOnPhCH_2O^-$, the hydroxymethyl alkoxide ion form of 3-hydroxy-4-nitrobenzyl alcohol; IBA, isobutyramide; RSSF, rapid-mixing stopped-flow; AU, absorbance unit.

0006-2960/87/0426-3058$01.50/0

active-site zinc (via direct coordination of DACA), the coenzyme (especially the positive charge on the nicotinamide ring of NAD^+), and the dipoles of residues in close proximity to the catalytic site. The highly red-shifted spectra of these DACA complexes are indicative of a strongly electron withdrawing catalytic site environment. This polar region of the site activates bound aldehyde for hydride attack via polarization of the carbonyl, and these same forces serve to activate alcohol for oxidation by increasing the concentration of the reactive species, alkoxide ion, via perturbation of the pK_a of bound alcohol to a lower value.

o- and *p*-nitrophenol and nitroaniline chromophores have been useful probes for investigating the catalytic properties of a variety of enzymes. For example, chromogenic substrates with *p*-nitrophenol or *p*-nitroaniline leaving groups have been of considerable use in the detection of intermediates in the hydrolytic reactions catalyzed by serine and cysteine proteases and by glycosidases. The 2-hydroxy-5-nitrobenzyl moiety (Burr & Koshland, 1964) has been used as a "reporter group" to study active-site environments. Using this reporter group, Frey et al. (1971) have demonstrated that, when it is incorporated into the catalytic site of acetoacetate decarboxylase, the pK_a of the phenolic hydroxyl is lowered by about 3.5 pK_a units, indicating that in comparison to water the site environment of this enzyme is highly polar.

In this series of papers, we introduce a new chromophoric LADH substrate, 3-hydroxy-4-nitrobenzaldehyde (HOnPhCHO). The ionizable hydroxyl group of the 3-hydroxy-4-nitrophenyl moiety makes this substrate a potentially interesting probe for investigating the electrostatic properties of the LADH substrate binding cleft during catalysis. As will be shown, the transient kinetic behavior of this substrate is characterized by the formation and decay of an enzyme-bound chemical intermediate. The kinetic behavior and spectroscopic properties of this intermediate indicate that the polarity of the substrate site varies enormously from the highly polar region of the active-site zinc to the essentially nonpolar binding cleft a few angstroms away.[2]

Experimental Procedures

Materials. Horse liver alcohol dehydrogenase (Boehringer Mannheim) was purified, and the active-site concentrations were determined as previously described (Dunn & Hutchinson, 1973). 3-Hydroxy-4-nitrobenzaldehyde (HOnPhCHO), 3-hydroxy-4-nitrobenzyl alcohol ($HOnPhCH_2OH$), and pyrazole (Aldrich) were vacuum sublimed before use. Concentrated stocks of HOnPhCHO and $HOnPhCH_2OH$ were made up in acetonitrile.

The coenzymes NAD^+ and NADH were obtained from Sigma Chemical Co. as the highest purity grades. Buffer solutions (chloride ion free) were prepared from crystalline salts by using doubly glass distilled water (Dunn et al., 1982). All concentrations reported refer to conditions after mixing in the stopped-flow spectrophotometer.

Instrumentation. Routine UV–visible spectra were obtained with either a Varian 635 or a Hewlett-Packard 8450A spectrophotometer. Single-wavelength transient kinetic studies were performed with a Durrum Model D110 stopped-flow spectrophotometer interfaced for on-line computer data acquisition and analysis (Dunn et al., 1979). Rapid-scanning stopped-flow spectroscopy was carried out on a modified Durrum Model D-110 stopped-flow spectrophotometer interfaced with a Princeton Applied Research (PAR) OMA-2 multichannel analyzer, 1218 controller, and 1412 photodiode array detector as described by Dunn et al. (1982) and Koerber et al. (1983).

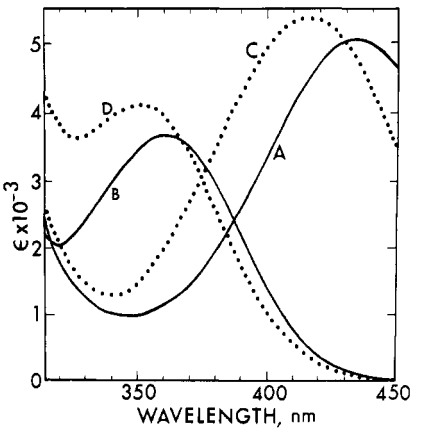

FIGURE 1: Comparison of spectra of 3-hydroxy-4-nitrobenzaldehyde at pH 8.75 (A) and at pH 4.03 (B) with spectra of 3-hydroxy-4-nitrobenzyl alcohol at pH 8.75 (C) and at pH 4.03 (D). Spectra were recorded at 25 ± 0.1 °C in 10 mM sodium pyrophosphate buffer (pH 8.75) or in 10 mM acetate buffer (pH 4.03).

Fluorescence spectroscopy on the stopped-flow instrument was carried out by detecting the emission at 90° to the exciting light through the appropriate filters. Auramine O fluorescence was measured by exciting at 450 nm (1-mm slit) and recording the emission fluorescence through a Schott Glass OG530 filter with a cutoff below 520 nm. For nucleotide fluorescence, excitation was at 330 nm and a 370-nm cutoff was used in emission (Schott Glass 65.1660).

Results

Liver alcohol dehydrogenase (LADH) catalyzes the interconversion of 3-hydroxy-4-nitrobenzaldehyde (HOnPhCHO) to the corresponding alcohol, 3-hydroxy-4-nitrobenzyl alcohol ($HOnPhCH_2OH$), with the concomitant interconversion of NADH and NAD^+. The stoichiometry of this reaction corresponds to the conversion of 1 mol of substrate/mol of coenzyme. Via steady-state kinetic studies (data not shown), the chemical course of the reaction has been verified by comparison of the UV–visible spectra of reactants and products with the spectra of authentic samples of HOnPhCHO and $HOnPhCH_2OH$.

The phenolic hydroxyl adjacent to the nitro group present in both HOnPhCHO and $HOnPhCH_2OH$ imparts chromophoric properties to these substrates that we exploit herein in determining the transient time course for the LADH-mediated interconversion. Figure 1 presents the UV–visible spectra of the ionized and neutral forms both for HOnPhCHO (spectra A and B, respectively) and for $HOnPhCH_2OH$ (spectra C and D, respectively). Ionization of the phenolic hydroxyl brings about large red shifts in the positions of the long-wavelength π,π^* transitions of these chromophores: ionization of HOnPhCHO (with pK_a = 6.0) to the delocalized phenoxide ion ($^-$OnPhCHO) shifts the λ_{max} from 360 to 433 nm, while ionization of $HOnPhCH_2OH$ (with pK_a = 6.9) to the corresponding phenoxide ion ($^-OnPh_2CHOH$) shifts the λ_{max} from 350 to 417 nm. At 428 nm, the extinction coefficients of $^-$OnPhCHO and $^-OnPh_2CHOH$ are identical. The relatively low energies of these electronic transitions make $^-$OnPhCHO and $^-OnPh_2CHOH$ relatively sensitive probes for UV–visible spectroscopic investigations of the physical and chemical events that occur during catalysis.

Rapid-Scanning Stopped-Flow Studies. The transient UV–visible spectral changes that occur when reaction is re-

[2] A preliminary account of a portion of this work has been presented in Dunn et al. (1986).

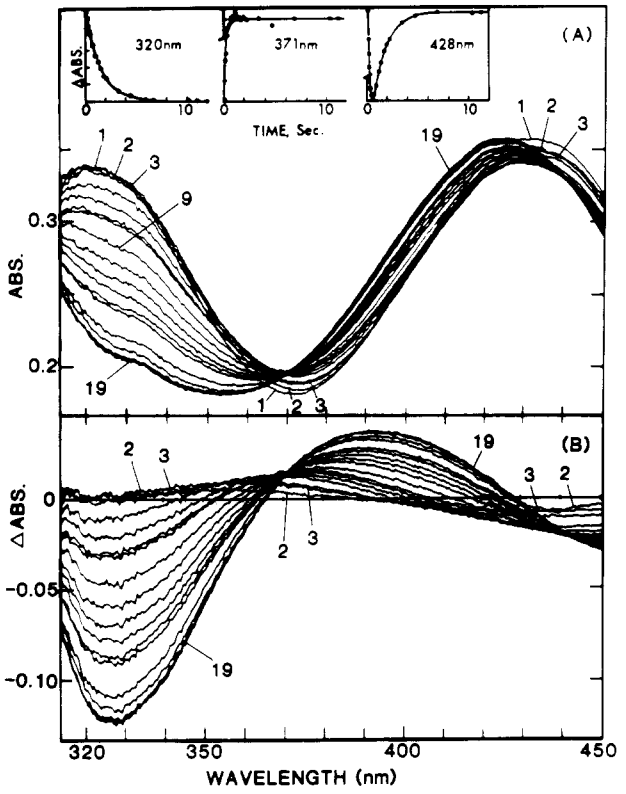

FIGURE 2: Time-resolved rapid-scanning stopped-flow (RSSF) spectra (A) and difference spectra (B) for reaction of the liver alcohol dehydrogenase–NADH complex with 3-hydroxy-4-nitrobenzaldehyde under single-turnover conditions at pH 8.75 and 25 ± 1 °C. The insets present the reaction time courses at 320 nm (a), at the 371-nm isoabsorbance point (b), and at 428 nm (where substrate and product have identical extinction coefficients) (c). Spectra were collected with a repetitive scanning rate of 8.605 ms/scan. At the longer times, delays of variable length were introduced between the scans to give the timing pattern indicated by the data points in the insets. Spectra are numbered consecutively. The difference spectra (B) were calculated by subtracting scan 1 from the other scans in (A). Conditions after mixing: [E] = 20 μN; [NADH] = 25 μM; [HOnPhCHO] = 40 μM; [pyrazole] = 20 mM; 10 mM sodium pyrophosphate buffer, pH 8.75. By inclusion of the potent inhibitor pyrazole reaction is limited to essentially a single turnover of enzyme sites.

stricted to a single turnover of sites are shown in Figure 2A. These rapid-scanning, stopped-flow (RSSF) data present the time-resolved spectral changes for the conversion of $^-$OnPhCHO to $^-$OnPhCH$_2$OH at pH 8.75. The presence of 20 mM pyrazole, a potent LADH inhibitor, limits reaction to essentially a single turnover of sites through the formation of a covalent adduct with enzyme-bound NAD$^+$ (McFarland & Bernhard, 1972; Eklund et al., 1982; Becker & Roberts, 1984). Since pyrazole binds only very weakly to the E(NADH) complex and since the reaction of pyrazole with the E(NAD$^+$) complex is rapid (McFarland & Bernhard, 1972), subsequent turnovers are precluded by the scavenging effects of pyrazole. The time-resolved spectra (Figure 2A), difference spectra (Figure 2B), and the accompanying single-wavelength time courses measured at 320, 371, and 428 nm (insets to Figure 2A) demonstrate that the single-turnover reaction is characterized by the formation and decay of an intermediate with spectral properties distinctly different from either $^-$OnPhCHO or $^-$OnPhCH$_2$OH.

The spectra in Figure 2 show the presence of two apparent isoabsorbance points[3] located at 371 and 441 nm that occur

[3] The term "isoabsorbance point" is used herein to designate those wavelengths where the absorbance remains constant (but nonzero) during one or more phases but not during all phases of the reaction.

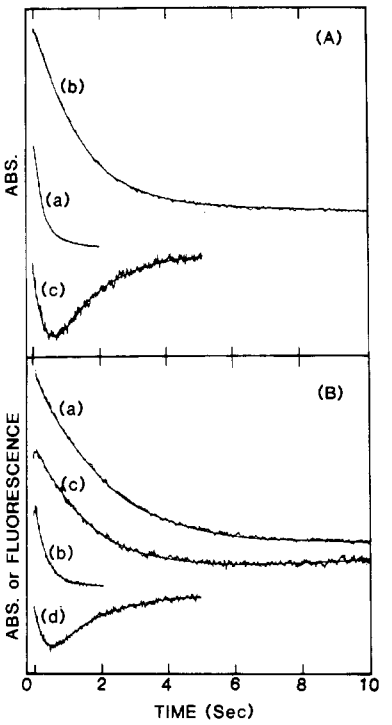

FIGURE 3: (A) Comparison of single-wavelength absorbance stopped-flow reaction time courses for disappearance of substrate (a) and NADH (b) and with intermediate formation and decay (c) for reaction of 3-hydroxy-4-nitrobenzaldehyde with the liver alcohol dehydrogenase–NADH complex under single-turnover conditions. The time courses shown are for (a) the disappearance of 3-hydroxy-4-nitrobenzaldehyde measured at the isoabsorbance point located at 460 nm, (b) 320 nm, and (c) 428 nm, the wavelength where substrate and product exhibit identical extinction coefficients. The best fit computer analyses of these time courses (see text) yielded the following observed rate constants and amplitudes: (a) 460 nm, λ_f = 2.9 s^{-1}, A_f = 0.015 AU; (b) 320 nm, λ_s = 0.73 s^{-1}, A_s = 0.036 AU; (c) 428 nm, λ_f = 3.3 s^{-1}, A_f = 0.017 AU; λ_s = 0.72 s^{-1}, A_s = 0.017 AU. Conditions after mixing: [E] = 10 μN; [NADH] = 100 μM; [HOnPhCHO] = 100 μM; [pyrazole] = 20 mM; 10 mM sodium pyrophosphate buffer, pH 8.75, 25 ± 1 °C. (B) Comparison of the time course for Auramine O displacement (a) with the time courses for substrate disappearance (b), NADH disappearance (c), and intermediate formation and decay (d) during the reaction of the E-(NADH, Auramine O) complex with 3-hydroxy-4-nitrobenzaldehyde. Conditions after mixing: [E] = 10 μN; [NADH] = 100 μM; [HOnPhCHO] = 100 μM; [pyrazole] = 20 mM; 10 mM sodium pyrophosphate buffer, pH 8.75; 25 ± 1 °C. The Auramine O fluorescence time course (a) was measured with λ_{ex} = 450 nm and λ_{em} > 520 nm in a solution containing 2 μM Auramine O. Traces b–d were collected in the absence of Auramine O with the same stock solutions of E, NADH, substrate, pyrazole, and buffer. The best fit computer analyses of these traces gave the following observed rate constants: (a) Auramine O fluorescence, λ_{em} > 520 nm, λ_s = 0.48 s^{-1}; (b) 460 nm, λ_f = 2.81 s^{-1}, A_{460} = 0.01 AU; (c) 320 nm, λ_s = 0.68 s^{-1}, A_{320} = 0.022 AU; (d) 428 nm, λ_f = 2.87 s^{-1}, A_{428} = 0.012 AU; λ_s = 0.76 s^{-1}, A_{428} = 0.014 AU. The solid, noise-free line superimposed on each trace is the theoretical best fit curve.

during the latter stages of the reaction. The intersection points are best seen in the difference spectra presented in Figure 2B. These difference spectra have been created by subtracting the first spectrum from the set (spectra 2–19). The time course for formation and decay of the intermediate is best seen at 428 nm (inset to Figure 2A). Comparison of this time course with the 371- and 320-nm time courses indicates that the absorbance changes at 371 nm (and at 441 nm, data not shown) measure only the fast relaxation, while the changes at 320 nm are dominated by the slow relaxation. The wavelengths at which the apparent isoabsorbance points occur were found to be substrate concentration dependent; for example, when the concentration of $^-$OnPhCHO is increased to 100 μM, the

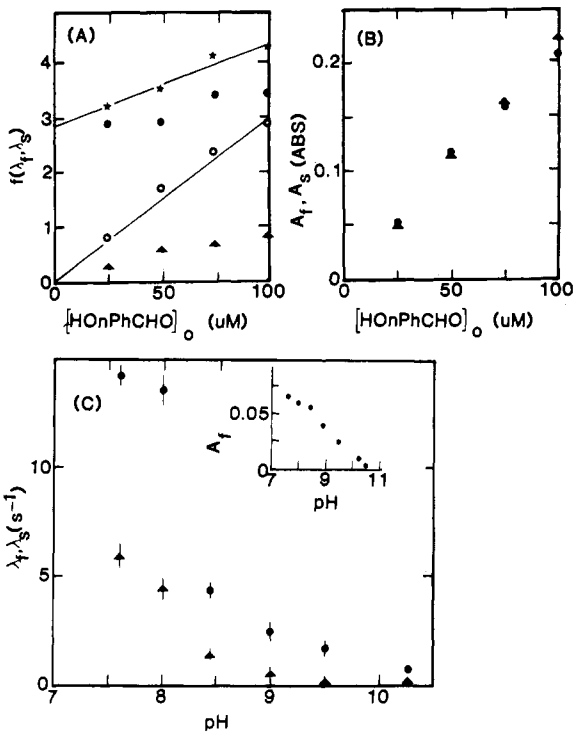

FIGURE 4: (A) Dependencies of λ_f (●), λ_s (▲), $\lambda_f + \lambda_s$ (★), and ($\lambda_f\lambda_s$) (○) on concentration of 3-hydroxy-4-nitrobenzaldehyde. The ordinate units are either s^{-1} (▲, ●, ★) or s^{-2} (○). (B) Dependence of the extrapolated amplitudes for intermediate formation, A_f (●), and decay, A_s (▲), measured at 428 nm, on the concentration of 3-hydroxy-4-nitrobenzaldehyde. The data for (A) and (B) were collected at pH 8.75 in 10 mM sodium pyrophosphate buffer at 25 ± 1 °C under experimental conditions similar to those described in the caption to Figure 3A. In (C), the pH dependencies of λ_f (●) and λ_s (▲) are shown. Buffers: 10 mM sodium phosphate (pH 7.5–8.0); 10 mM sodium pyrophosphate (pH 8.05–9.5); 10 mM sodium carbonate (pH 10.3–10.5). The inset summarizes the pH dependence of the extrapolated amplitude for intermediate formation.

long-wavelength crossover point shifts to 460 nm (viz., the single-wavelength time course presented in Figure 3A). Extensive investigation of the reaction via single-wavelength stopped-flow measurements as a function of wavelength and substrate concentration and with quantitative treatment of the rate data via computer analysis gave no evidence for any additional relaxations in the reaction. Typical single-wavelength time courses are shown in Figure 3A for the wavelengths 320, 428, and 460 nm. Under these conditions, the fast and slow relaxations (when analyzed as single, first-order decay processes) have rate constants of 2.9 s^{-1} (λ_f, trace a) and 0.73 s^{-1} (λ_s, trace b), in close agreement with the best fit rate constants for the biphasic time course (3.3 s^{-1} and 0.72 s^{-1}, trace c).

Concentration Dependencies of Rates and Amplitudes. The effect of substrate concentration on the production and decay of the intermediate was investigated at 428 nm, the isosbestic point of $^-$OnPhCHO and $^-$OnPh$_2$CHOH at pH 8.75. The observed relaxation rate constants (λ_f and λ_s) and amplitudes (A_f and A_s) were determined by computer fitting of the reaction time courses to the rate expression

$$A_t = A_\infty - A_f \exp(-\lambda_f t) + A_s \exp(-\lambda_s t) \quad (1)$$

where A_t and A_∞ are respectively the absorbances at time t and t_∞.

Figure 4 summarizes the rate data from experiments where LADH and NADH were mixed in the single-wavelength stopped-flow apparatus with Pyr and varying concentrations of HOnPhCHO. The results (Figure 4A) show that λ_s and λ_f are both concentration dependent. The amplitudes, A_f and A_s (which represent the expected amplitude of one phase in the absence of the other), both show dependencies that are linear with respect to the concentration of substrate (Figure 4B).

The simplest kinetic scheme that is consistent with the concentration dependencies exhibited by λ_f and λ_s is one in which the E(NADH) complex binds substrate S to form an intermediate E(X) that releases product P. The pathway shown in eq 2 formally predicts three relaxations. However,

$$\begin{array}{l} E(NADH) + S \underset{k_{-1}}{\overset{k_1}{\rightleftharpoons}} E(X) \underset{k_{-2}}{\overset{k_2}{\rightleftharpoons}} E(NAD^+) + P \\ \qquad\qquad\qquad\qquad\qquad\quad \Big\downarrow k_3 \\ \qquad\qquad\qquad\qquad\qquad\quad E(NAD\text{-}Pyr) \end{array} \quad (2)$$

if $k_3[Pyr] \gg k_1[S] + k_{-1}$ and $\gg k_2 + k_{-2}[P]$, then eq 2 can be approximated by a two-step reaction (eq 3) in which the second step is made quasi-irreversible by the reaction with pyrazole (eq 4). This simplification is justified by the experiments of McFarland and Bernhard (1972), which established that, in the presence of 20 mM Pyr, $k_3[Pyr] \geq 100\ s^{-1}$, a value that is much greater than either λ_f or λ_s.

$$E(NADH) + S \underset{k_{-1}}{\overset{k_1}{\rightleftharpoons}} E(X) \underset{k_{-2}}{\overset{k_2}{\rightleftharpoons}} P + E(NAD^+) \quad (3)$$

$$E(NAD^+) + Pyr \xrightarrow{k_3} E(NAD^+\text{–}Pyr) \quad (4)$$

Under the experimental conditions employed in these studies, $[S]_0 \gg [E(NADH)]_0$; consequently, the pseudo-first-order approximation is valid for the bimolecular step, and the system depicted in eq 3 can be treated as two pseudo-first-order relaxations. Equations 5 and 6 (Bernasconi, 1976)

$$\lambda_f + \lambda_s = k_1[S] + k_{-1} + k_2 \quad (5)$$

$$\lambda_f\lambda_s = k_1k_2[S] \quad (6)$$

define the relationships between the observed relaxation rates λ_f and λ_s and the rate constants that describe intermediate formation and decay. Equations 5 and 6 predict that a plot of $\lambda_f + \lambda_s$ vs. [S] will be linear with a slope = k_1 and an intercept = $k_{-1} + k_2$, while a plot of $\lambda_f\lambda_s$ vs. [S] will be linear with a slope = k_1k_2. The data presented in Figure 4A indicate that these predictions are met with the HOnPhCHO system: the plot of $\lambda_f + \lambda_s$ vs. [S] is linear [slope = (1.5 ± 0.2) × 10^4 M^{-1} s^{-1}; intercept = 2.9 ± 0.2 s^{-1}]; the plot of $\lambda_f\lambda_s$ vs. [S] is also linear (slope ~ 3 × 10^4 M^{-1} s^{-2}). Note that since over the concentration range investigated λ_f and λ_s are similar in magnitude, the separation of the decay constants is not easy. Nevertheless, the slope and intercept data provide the following estimates for the rate constants in eq 3: k_1 = 1.5 × 10^4 M^{-1} s^{-1}, k_{-1} = 0.9 s^{-1}, and k_2 = 2.0 s^{-1}.

Proton Uptake Studies. The uptake of protons from solution during the reaction of HOnPhCHO with the E(NADH) complex was investigated according to the method of Dunn (1974) under conditions that limit reaction to a single turnover ([NADH] < [E] < [HOnPhCHO]). This method employs a pH indicator (thymol blue) both as the buffer and as the signal for monitoring the time course for proton uptake or release at pH 8.75. In these experiments, a solution containing 20 μN enzyme and 15 μM NADH (the limiting reactant) was premixed in 100 mM Na_2SO_4 with 50 μM thymol blue, adjusted to pH 8.75 with NaOH, and then mixed in the stopped-flow apparatus with a 40 μM HOnPhCHO solution containing 100 μM Na_2SO_4 and 50 μM thymol blue (also adjusted to pH 8.75). The proton uptake time course (mea-

Table I: Summary of Rate Constants for the Equine Liver Alcohol Dehydrogenase Catalyzed Reaction of 3-Hydroxy-4-nitrobenzaldehyde with NADH

experiment	signal (nm)	λ_f (s^{-1})	$(\lambda_f^H/\lambda_f^D)$	λ_s (s^{-1})	$(\lambda_s^H/\lambda_s^D)$
^2H isotope effects[a]					
NADH	abs 428	3.3 ± 0.3	1.3 ± 0.15	0.73 ± 0.1	1.4 ± 0.24
NADD	abs 428	2.5 ± 0.3		0.51 ± 0.1	
NADH	abs 320			0.70 ± 0.05	2.0 ± 0.11
NADD	abs 320			0.35 ± 0.03	
NADH	abs 460[b]	2.9 + 0.15	1.0 ± 0.07		
NADD	abs 440[b]	3.0 ± 0.15			
comparison of NADH fluorescence and absorbance time courses[c]	abs 428	3.65 ± 0.3		0.49 ± 0.1	
	abs 320			0.34 ± 0.05	
	λ_{ex} 330; λ_{em} >370			0.35 ± 0.05	
Auramine O displacement studies[d]	abs 428	2.9 ± 0.3		0.76 ± 0.2	
	abs 320			0.68 ± 0.05	
	λ_{ex} 450; λ_{em} >520			0.48 ± 0.05	
proton uptake studies[e]	abs 428	2.5 ± 0.3		0.53 ± 0.1	
	abs 620	2.1 ± 0.3		0.75 ± 0.2	

[a] Conditions after mixing: [E] = 10 μN; [NADH] or [NADD] = 100 μM; [HOnPhCHO] = 100 μM; [Pyr] = 20 mM; 10 mM sodium pyrophosphate buffer, pH 8.75; 25 ± 1 °C. [b] Under these experimental conditions, the isoabsorbance point shifts from 460 to 440 nm when NADD is substituted for NADH. [c] Conditions after mixing: [E] = 20 μN; [NADH] = 25 μM; [HOnPhCHO] = 40 μM; [Pyr] = 10 mM; 10 mM sodium pyrophosphate buffer, pH 8.75; 25 ± 1 °C. [d] The absorbance time courses were measured in the absence of Auramine O under the same conditions described in footnote *a*. The Auramine O fluorescence time course was measured after the addition of Auramine O (2 μM after mixing). [e] For 620-nm data, conditions after mixing: [E] = 20 μN; [NADH] = 15 μM; [HOnPhCHO] = 40 μM; [thymol blue] = 50 μM (both syringes contained 50 μM thymol blue); 0.1 M sodium sulfate; pH 8.75; 25 ± 1 °C. The 428-nm data were measured in the absence of thymol blue.

sured at 620 nm) was found to be biphasic with decay constants. $\lambda_f^{H^+} = 2.1\ s^{-1}$ and $\lambda_s^{H^+} = 0.75\ s^{-1}$ and similar amplitudes in each phase (Table I). A control experiment employing the same concentrations of reactants in which the 428-nm time course for intermediate formation and decay was monitored in the absence of thymol blue yielded a biphasic time course with similar decay constants. These experiments indicate that approximately the same amount of hydrogen ion is taken up in each phase of the reaction.

Effect of pH on the Reaction. Single-wavelength stopped-flow studies were carried out in the pH region 7.0–10.5. These studies show that both λ_f and λ_s are pH-dependent processes. Figure 4D summarizes the effects of pH on these relaxations. As the pH is lowered, both λ_f and λ_s increase and the ratio λ_f/λ_s decreases. The inset to Figure 4C shows that the extrapolated amplitude of the slow phase A_s increases with decreasing pH and appears to level off in the region of pH 7. These amplitude and rate studies establish that, at high pH, the amount of intermediate that accumulates is very small; decreasing pH results in the accumulation of increased amounts, and this increase plateaus as pH 7 is approached.

Nucleotide Fluorescence Studies and Deuterium Isotope Effects. From inspection of Figures 1 and 2, it is reasonable to assume that the spectral changes due to oxidation of bound NADH make a substantial contribution to the absorbance changes in the 320-nm region of the spectrum. However, the absorbance changes from other species may make significant contributions to this region of the spectrum. Consequently, additional experiments were undertaken to provide an experimental basis for assigning λ_f and λ_s to specific events in catalysis. Therefore, nucleotide fluorescence and deuterium kinetic isotope studies were performed to identify the hydride-transfer step.

When excited by light in the 320–360-nm region, the E-(NADH) binary complex and many ternary complexes containing NADH exhibit strong fluorescence from the 1,4-dihydronicotinamide moiety, while the high and low pH forms of substrate and product do not fluoresce under these conditions. Therefore, stopped-flow experiments were undertaken to determine the time course for NADH oxidation. Analysis of the nucleotide fluorescence emission time course showed a single relaxation with a first-order decay constant (Table I) that is identical (within the limits of experimental error) with λ_s. Hence, the hydride transfer process must occur in λ_s.

The effect of substituting deuterium for the (4*R*)-4-hydrogen of NADH on the time course of the reaction was studied via single-wavelength stopped-flow methods in the absorbance mode. When (4*R*)-4-deuterio-NADH (NADD) is substituted for NADH, the amount of intermediate that accumulates decreases and the location of the isoabsorbance points change. By following the reaction at 320 (slow phase), 428 (both phases), and 460 (NADH, fast phase), or 440 nm (NADD, fast phase), it was possible to determine the isotope effect on each phase (see Table I). These data establish that λ_s is subject to a small primary isotope effect, $\lambda_s^H/\lambda_s^D = 2.0$ (Table I), while the effect on λ_f is small. Comparison of isotope effects at 100 and 25 μM HOnPhCHO shows that the isotope effect on λ_s is insensitive to this variation in substrate concentration.

Auramine O Displacement Studies. The fluorescence of Auramine O when bound to the substrate binding site of LADH is greatly enhanced (Conrad et al., 1970). Kinetic studies of Sigman and Glazer (1972) and Andersson et al. (1981) have established that the forward and reverse rate constants for the binding of Auramine O both to LADH and to LADH–coenzyme binary complexes are rapid relative to λ_f and λ_s. Consequently, Auramine O is particularly well suited for use as a fluorophoric indicator of ligand binding to the LADH substrate binding site. Under conditions where the fraction of LADH sites occupied by Auramine O is relatively small, the attenuation of the observed rate of ligand binding due to competition with Auramine O will be small. Thus to a good first approximation, the rate of Auramine O displacement will be determined by the rate of accumulation of bound substrate species (Bernasconi, 1976). The traces presented in Figure 3B compare the fluorescence changes for the displacement of Auramine O by $^-$OnPhCHO at pH 8.75 (trace a) with the transient absorbance changes at 320 (trace b), 428 (trace c), and 460 nm (trace d) during a single turnover of $^-$OnPhCHO to $^-$OnPhCH$_2$OH. The time course for the displacement of Auramine O is well described by the rate expression for a single-exponential decay with an apparent first-order rate constant of 0.48 s^{-1}. No evidence for another phase could be found. From comparison of the rate constants

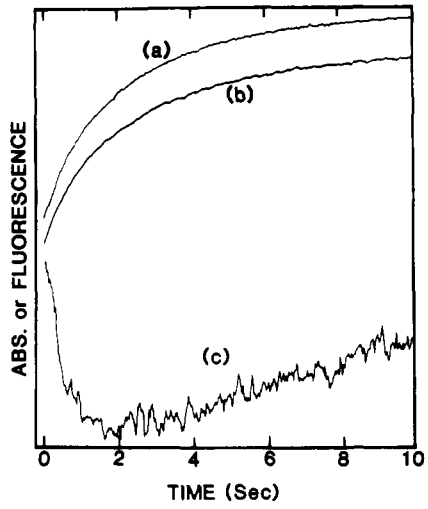

FIGURE 5: Comparison of the NADH (a) and protein (b) fluorescence time courses with the absorbance time course for intermediate formation and decay (c) in the reaction of 3-hydroxy-4-nitrobenzyl alcohol with the liver alcohol dehydrogenase–NAD^+ complex. Nucleotide fluorescence (λ_{ex} = 330 nm) and protein fluorescence (λ_{ex} = 290 nm with reemission as nucleotide fluorescence) were measured as the light emitted at $\lambda > 370$ nm. Reaction was limited to approximately a single turnover by the inclusion of isobutyramide (see text). Conditions after mixing: [E] = 16.7 μN; $[NAD^+]$ = 259 μM; $[HOnPhCH_2OH]$ = 100 μM; [isobutyramide] = 100 mM; 10 mM sodium pyrophosphate buffer, pH 8.75; 25 ± 1 °C. Best fit rate constants: (a) λ_f^* = 8.9 s^{-1}, λ_s^* = 1.9 s^{-1}; (b) λ_f^* = 8.5 s^{-1}, λ_s^* = 1.8 s^{-1}; (c) λ_f^* = 8.8 s^{-1}, λ_s^* = 1.2 s^{-1}.

derived from the time courses in Figure 3B (see Table I also), it is clear that the apparent rate of Auramine O displacement (0.48 s^{-1}) is nearly identical with the value of λ_s (0.68 s^{-1}, measured at 320 nm) and quite different from the value of λ_f (3.0 s^{-1}, measured at 460 nm). Consequently, it appears that displacement of Auramine O and the disappearance of NADH are concomitant processes. (The slightly lower value of the Auramine O displacement rate very likely has its origins in the competition between Auramine O and substrate.)

Pre-Steady-State Kinetics of 3-Hydroxy-4-nitrobenzyl Alcohol Oxidation. In the presence of high concentrations of isobutyramide (IBA), the steady-state rate of the LADH-catalyzed oxidation of alcohols is strongly inhibited via formation of the inhibitory E(NADH, IBA) ternary complex, while the pre-steady-state phase of the reaction is unaffected (Luisi & Bignetti, 1974; Kvassman & Pettersson, 1978). Through use of the IBA method, we have examined the kinetics of $^-OnPhCH_2OH$ oxidation (Figure 5) by monitoring the production of NADH, both via direct emission of fluorescence from the bound coenzyme and via fluorescence energy transfer from the protein tryptophan residues to bound NADH, and also by monitoring the absorbance changes at 428 nm (the wavelength where $^-OnPhCH_2OH$ and $^-OnPhCHO$ have the same extinction coefficient). The time courses measured by these signals (Figure 5) are all biphasic. Comparison of the computer-generated best fit rate constants establishes that the same two relaxations are detected with each signal. Under the conditions of Figure 5, the fast relaxation, λ_f^*, has an apparent rate of 8.7 ± 0.2 s^{-1} and the slow relaxation, λ_s^*, has an apparent rate of 1.8 ± 0.12 s^{-1}.

Steady-State Kinetics. Because the preceding experiments on aldehyde reduction indicate that λ_s is limited by hydride transfer in the single turnover reaction, it then should be possible that the same process is limiting in the steady-state reaction. Steady-state analyses at pH 8.75 in 0.1 M pyrophosphate buffer show that the K_m for 3-hydroxy-4-nitrobenzaldehyde is 60 μM and $k_{cat} \simeq 0.3$ s^{-1}. If the inverse square roots of the amplitude values taken from Figure 4B are plotted vs. 1/[S], then an estimate of K_m can be obtained from the resulting plot by dividing the slope by the y intercept (Laidler & Bunting, 1973). This treatment of the data also yields a value of ~60 μM for K_m.

The steady-state rate was tested for an isotope effect by comparing NADH or NADD (100 μM) in solutions containing a saturating concentration of HOnPhCHO (300 μM) and LADH (0.75 μN) in 10 mM phosphate buffer at pH 8.75. The reaction was followed at 475 nm, the high-wavelength side of the substrate peak ($\Delta\epsilon_{475} = 1 \times 10^3$ M^{-1} cm^{-1}), so that the high background absorbance at the λ_{max} could be avoided. The rate of change in absorbance (absorbance unit per minute) was 0.31 AU/min (NADH) and 0.18 AU/min (NADD), giving k_{cat} values for NADH and NADD of 0.7 s^{-1} and 0.4 s^{-1}, respectively, and an isotope effect of $k_{cat}^H/k_{cat}^D = 1.7$. These values are of the same order of magnitude as the rate of the slow phase detected in the transient experiments. When the concentration of NADD was doubled, the same steady-state rate was observed. Consequently, the decreased rate is not due to differential binding of NADD. When the steady-state reaction is monitored by the absorbance changes at 320 nm, where the oxidation of NADH dominates the spectrum, the same isotope effect of 1.7 is obtained.

Discussion and Conclusions

At pH above 7, the reaction of 3-hydroxy-4-nitrobenzaldehyde with the E(NADH) binary complex is shown herein to occur via a transient chemical intermediate, E(X). The RSSF data and single-wavelength time courses presented in Figures 2 and 3 indicate that at pH 8.75 the intermediate has a spectrum that is remarkably different from that of the reactant or product.

In order to assign physicochemical properties to the intermediate, the following experimental findings must be explained. (1) Only two kinetic relaxations, λ_f and λ_s, are detected under single turnover conditions (viz., Figures 2 and 3 and Table I). (2) The RSSF data (Figure 2 and data not shown) establish the existence of two isoabsorbance points during λ_s. The positions of these points depend on the concentration of substrate and shift when deuterium is substituted for the (4*R*)-4-hydrogen of NADH. (3) As is evident in Figure 4, both λ_f and λ_s show some dependence on [S]. (4) The slow relaxation is subject to a small primary isotope effect (λ_s^H/λ_s^D = 2.0) which is unaffected by changing the substrate concentration from 25 to 100 μM, whereas there is little or no isotope effect on the fast relaxation (Table I). (5) When NADD is substituted for NADH, the maximum amount of intermediate that accumulates is decreased, and the time at which the maximum amount forms is increased. (6) The time course for the displacement of Auramine O is characterized by a single relaxation with rate λ_s (Figure 3B and Table I). (7) Both λ_f and λ_s increase with decreasing pH, and the extrapolated amplitude for the formation of E(X) also increases as the pH is decreased (inset to Figure 4C). (8) The time course for H^+ uptake occurs in two phases with apparent rates equal to λ_f and λ_s (Table I). The amplitudes of these two phases are similar. (9) Steady-state kinetic studies indicate $k_{cat} \simeq \lambda_s$ and K_m = 60 μM; k_{cat} is also subject to a primary isotope effect $k_{cat}^H/k_{cat}^D = 1.7$).

Inferences about the Nature of E(X). Because the displacement of Auramine O occurs with a rate essentially identical with λ_s, we are compelled to conclude that the slower process (λ_s) precedes the faster process (λ_f). This conclusion is supported by the finding that the primary isotope effect on λ_s decreases the maximum amount of intermediate formed and

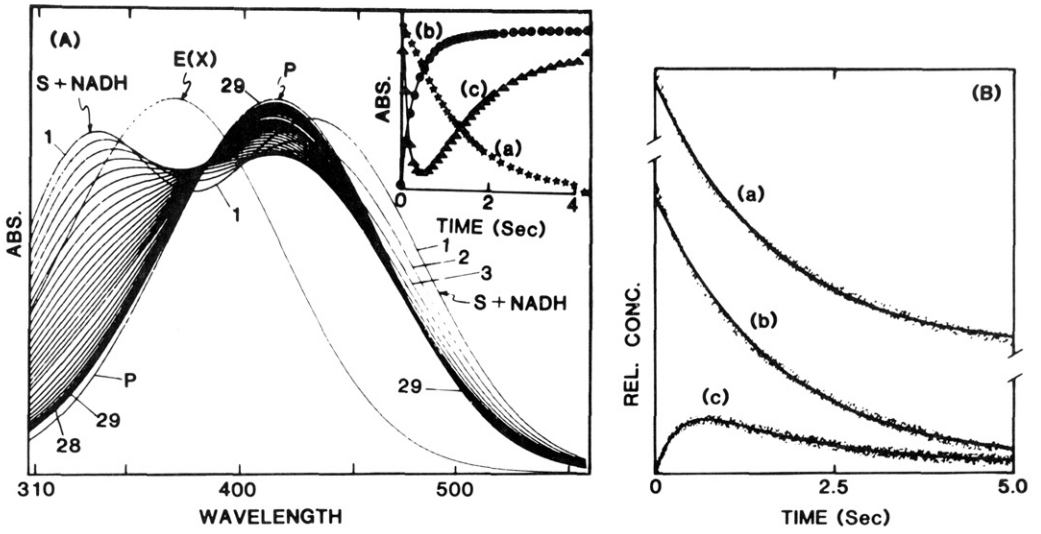

FIGURE 6: (A) Simulation of rapid-scanning stopped-flow spectra for reaction of 3-hydroxy-4-nitrobenzaledhye with the liver alcohol dehydrogenase–NADH complex. Spectra of $^{-}$OnPhCHO, $^{-}$OnPhCH$_2$OH, the intermediate E(S), and NADH were simulated as Gaussian-shaped electronic transitions. The inset shows single-wavelength time courses measured at 320 nm (a), the isoabsorbance point located at 385 nm (b), and the isoabsorbance point located at 427 nm (the wavelength where substrate and product exhibit identical extinction coefficients). The amplitudes of these signals have been normalized to assist visual comparison. The last data point in each time course is the t_∞ value. The time course for reaction was modeled as the two-step sequence shown in Scheme II (see text) with $k_{12} = 3$ s^{-1}, $k_{21} = 2$ s^{-1}, and $k_{23} = 4$ s^{-1}. As is evident in this simulation, when the intermediate is assigned a spectrum similar to that of HOnPhCH$_2$OH (viz., Figure 1, spectrum D), then the computer-simulated time-resolved spectra give a pattern that is similar to the pattern observed in the RSSF time course shown in Figure 2A. (B) Computer simulation of the theoretical time courses for the disappearance of $^{-}$OnPhCHO (a) and E(NADH) (b) and the formation and decay of $E(NAD^+, HOnPhCH_2O^-)$ (c), at pH 8.75, as predicted by Scheme I for the rate constants and concentrations described in the text. The digital computer simulations of the kinetic time courses for each species in Scheme I were carried out by using the fourth-order Runge–Kutta approximation algorithm. The theoretical time courses were then altered by the introduction of random noise (±2%) and subjected to analysis to determine the best fit apparent rate constants, assuming that time courses a and b can be described as first-order decays, $X = X_\infty + X_0 \exp(-k_s t)$, and that time course c can be described as the difference between two exponential processes, $X = F[\exp(-k_f t) - \exp(-k_s t)]$, where X is the concentration of the species at any time t, X_∞ is the concentration at infinite time, F is a constant, and X_0 is the total amount of species X that undergoes reaction. The best fit analyses give the following apparent contants: (a) $k_s = 0.60$ s^{-1}; (b) $k_s = 0.60$ s^{-1}; (c) $k_f = 3.25$ s^{-1}; $k_s = 0.53$ s^{-1}. The solid noise-free lines drawn through the traces are the computer-generated theoretical best fits based on the above assumptions.

increases the time at which the maximum amount accumulates. If λ_f were related to the first process, then a slowing of λ_s by substitution of NADD for NADH would increase the amount of intermediate formed. In fact, it is found that as the difference in the decay constants of the phases increases, the amount of intermediate decreases, leading to the conclusion that the slower process precedes the faster one. These conclusions are further substantiated by the finding that the nucleotide fluorescence changes occur in λ_s and that the 320-nm absorbance changes are dominated by λ_s. Consequently, the intermediate must be a species formed after the hydride-transfer step, and thus we conclude that E(X) is a ternary complex consisting of enzyme, NAD$^+$, and some form of alcohol.

Since λ_s precedes λ_f, this substrate provides an uncommon set of circumstances where intermediate formation is slower than intermediate decay, but the rates of λ_f and λ_s are close enough to allow detectable amounts of intermediate to accumulate. Because the displacement of Auramine O occurs at the rate λ_s, substrate binding must be an unfavorable, rapid preequilibrium step that precedes hydride transfer.[4] If substrate binds only weakly in the E(NADH, S) ternary complex, then the concentration of this ternary complex will be small and the relaxation for Auramine O displacement due to the substrate binding step will have a negligible amplitude. Hence, the displacement of Auramine O will occur at the rate of accumulation of E(X). As will be shown below, these properties of the system explain the insensitivity of the isotope effect to changes in [S].[4]

The spectral changes (Figure 2) that characterize intermediate formation at pH 8.75 indicate that the intermediate has a much lower extinction coefficient at 428 nm than that of the substrate or product. Because the decay constants are of similar magnitude and, more importantly, the slow phase precedes the fast phase, the concentration of the intermediate is much smaller than the total concentration of enzyme sites (see the simulation in Figure 6B). According to eq 3, the maximum proportion of intermediate that accumulates is given by the relationship (Bernasconi, 1976; Frost & Pearson, 1961)

$$\beta_{max} = (k_1/\lambda_f)\kappa^{\kappa/(1-\kappa)} \qquad (7)$$

where $\kappa = \lambda_s/\lambda_f$ and k_1 is the rate constant for intermediate formation (viz., eq 3, using k_1 predicted from eq 5). When the observed maximum absorbance difference at 428 nm due to intermediate formation is plotted vs. the maximum proportion of intermediate formed, β_{max}, the slope of the resulting linear plot (data not shown) is $\Delta\epsilon_{428}[E(NADH)]_0 = 0.037[E(NADH)]_0 = 10\ \mu M$, and therefore, $\Delta\epsilon_{428} \simeq 3.7 \times 10^3$ M^{-1} cm^{-1}. Because no new red-shifted peak appears in the RSSF studies (data not shown), this value indicates that the ϵ_{428} of the intermediate is $\sim 1.3 \times 10^3$ M^{-1} cm^{-1}. This change in ϵ_{428} must be the consequence of a large blue shift in the spectrum of the chromophore. Since the long-wavelength spectral bands of substrate and product at pH 8.75 are

[4] Clearly, the presence of a primary isotope effect on λ_s rules out mechanisms that depend on a slow, rate-limiting specific rate constant for the binding of substrate. The detection of a single phase in the Auromine O displacement time course with rate λ_s eliminates from consideration any mechanism that proposes a fast step to form a ternary complex, E(NADH, HOnPhCHO), in which substrate is tightly bound. Similarly, since the primary isotope effect is independent of substrate concentration, mechanisms that invoke similar rates for ternary complex formation [to form E(NADH, HOnPhCHO)] and for hydride transfer also must be rejected.

Scheme I

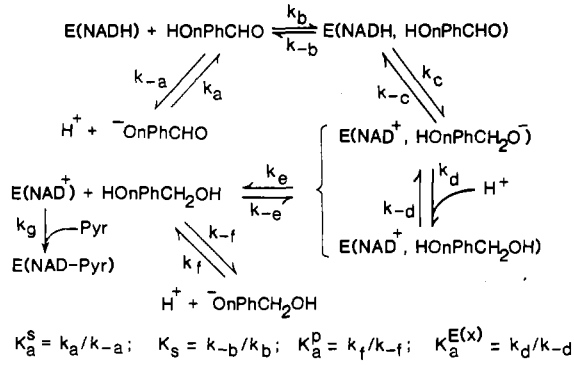

$K_a^S = k_a/k_{-a}$; $K_S = k_{-b}/k_b$; $K_a^P = k_f/k_{-f}$; $K_a^{E(x)} = k_d/k_{-d}$

due to the *o*-nitrophenoxide ion chromophore and since these spectral bands are shifted to shorter wavelengths in the neutral species (Figure 1), we propose that the blue-shifted intermediate is a species in which the phenolic group is neutral.

Kinetic Mechanism for Reduction of 3-Hydroxy-4-nitrobenzaldehyde. The constraints imposed by the above-described findings and inferences restrict the possible mechanisms to a relatively small set. If reaction with HOnPhCHO proceeds via the interconversion of ternary complexes, i.e.

$$E(NADH, HOnPhCHO) \rightleftharpoons E(NAD^+, HOnPhCH_2O^-)$$

as has been demonstrated for other LADH substrates (Dunn & Hutchison, 1973; Koerber et al., 1983; Kvassman et al., 1981; Cedergren-Zeppezauer et al., 1982; Sartorius et al., 1987; Dunn, 1985), then we propose Scheme I is a mechanistically sound explanation for the LADH-catalyzed reduction of 3-hydroxy-4-nitrobenzaldehyde by NADH in the pH region 7–10.5. In Scheme I, K_a^S, K_a^P, and $K_a^{E(X)}$ are the ionization constants, respectively, for the phenolic hydroxyls of HOnPhCHO and $HOnPhCH_2OH$ and the aliphatic hydroxyl of bound X. This scheme proposes that binding and reaction occur exclusively via the neutral phenolic hydroxyl form of the substrate. If all proton-transfer steps and all binding steps in Scheme I are rapid processes in comparison to λ_f and λ_s, then Scheme I can be approximated by the two-step sequence shown in Scheme II, where $k_{12} = k_c[S_T]/(K + [S_T])$, $K = (k_{-b}/k_b)(k_a/k_{-a}) = K_s[(K_a^S + [H^+])/[H^+]]$, $[S_T]$ = the total amount of substrate initially present, and $k_{23} = k_e[H^+]/(K_a^{E(X)} + [H^+])$.

Scheme II

$$E(NADH, HOnPhCHO) \underset{k_{21}}{\overset{k_{12}}{\rightleftharpoons}} E(NAD^+, HOnPhCH_2O^-) \xrightarrow{k_{23}} E(NAD\text{–}Pyr) + {}^-OnPhCH_2OH$$

It then follows that

$$\lambda_f + \lambda_s = k_{12} + k_{21} + k_{23} = k_c[S_T]/(K + [S_T]) + k_{21} + k_e[H^+]/(K_a^{E(X)} + [H^+]) \quad (8)$$

and

$$\lambda_f\lambda_s = k_{12}k_{23} = \{k_c[S_T]/(K + [S_T])\}\{k_e[H^+]/(K_a^{E(X)} + [H^+])\} \quad (9)$$

According to eq 8 and 9, plots of $\lambda_f + \lambda_s$ and $\lambda_f\lambda_s$ vs. $[S_T]$ should saturate when $[S_T] \gg K$. However, at low $[S_T]$ when $[S_T] \ll K$, $\lambda_f + \lambda_s \simeq k_c[S_T]/K + k_{21} + k_{23}$, and $\lambda_f\lambda_s \simeq k_ck_{23}[S_T]/K$. Hence, in agreement with Figure 4A, both functions become proportional to $[S_T]$ when the concentration of S_T is low.

According to Schemes I and II, the sluggish rate of hydride transfer (i.e., λ_s) is the result of two effects: (1) the relatively weak affinity of HOnPhCHO for the E(NADH) binary complex ensures a low (steady-state) level of E(NADH, HOnPhCHO) and (2) the low pK_a for the ionization of HOnPhCHO to ⁻OnPhCHO ($pK_a = 6$) keeps the concentration of the reactive form of the substrate at a low steady-state value at pH >7. If k_b is assumed to be similar to values measured for other substrates (i.e., for DACA, $k_b = 4 \times 10^7$ M^{-1} s^{-1}; Dunn & Hutchinson, 1973), then for $[S_T] = 2 \times 10^{-4}$ M, the pseudo-first-order rate constant for the binding of HOnPhCHO at pH 8.75 can be estimated as $k_{obsd} = [HOnPhCHO]k_b = (2.58 \times 10^{-7}\ M)(4 \times 10^7\ M^{-1}\ s^{-1}) = 10.3\ s^{-1}$, a value that (under these experimental conditions) would exceed both λ_f and λ_s (Table I).

In the general case, K_m can be shown to be given by the relationship $K_m = [E][S]/\{[E(S)] + [E(P)] + \sum_{i=1}^{n}[E(X_j)]\}$, where [E] and [S] are the steady-state concentrations of E and S, $E(X)_j$ is the *j*th chemical intermediate along the path, and E(S) and E(P) are the substrate and product Michaelis complexes of S and P, respectively (Dunn & Bernhard, 1974). It follows that when intermediates other than E(S) make a significant contribution to the steady-state distribution of intermediates, then $K_m < K$. Since such intermediates accumulate in this system (vide infra), then $K_m = 60\ \mu M < K$, and our experimental conditions preclude the accumulation of detectable amounts of E(NADH, S).[4]

Computer Simulations. Our RSSF studies demonstrate that the locations of the two isoabsorbance points seen in Figure 2 vary with changes in the concentration of substrate and shift when NADD is substituted for NADH. If the system is adequately described by Scheme II, then computer simulation of the RSSF traces by constraining reaction to occur via Scheme II should reproduce these spectroscopic features. Such simulations are shown in Figure 6A for the case where the reactant and product have spectra similar to ⁻OnPhCHO and $^-OnPhCH_2OH$, respectively, and the intermediate has a spectrum similar to $HOnPhCH_2OH$. The spectra were modeled as Gaussian curves with appropriate bandwidths, λ_{max}, and ϵ values and with rate constants $k_{12} = 3\ s^{-1}$, $k_{21} = 2\ s^{-1}$, and $k_{23} = 4\ s^{-1}$. Note that these simulated RSSF spectra exhibit clean isoabsorbance points in the slow phase that are located above and below the λ_{max} of reactant and product. Variation of the rate constants in the model shifts the location of these intersection points (data not shown).

To test whether or not the above-postulated relationships between concentrations and rate constants actually reduce the complexity of Scheme I to the system of two relaxations described by Scheme II, we carried out digital computer simulations to generate theoretical single-wavelength time courses (viz., Figure 6B) for the appearance and/or decay of all the species depicted in Scheme I. The assumptions used in the simulation are as follows: (a) Since NADH and enzyme are premixed prior to mixing with substrate, the simulation assumes all enzyme is initially in the form of E(NADH). (b) All proton transfers between solvent and substrate or product are assumed to be rapid relative to all other steps in Scheme I. (c) If HOnPhCHO is the form of substrate that binds and reacts, then the apparent second-order rate constant for substrate binding $k_b' = k_b[H^+]/(K_a^S + [H^+])$. Assuming a value of k_b between 1×10^7 and 4×10^7 M^{-1} s^{-1} and $K_a^S = 1 \times 10^{-6}$ M, then at pH 8.75 $k_b' = 2 \times 10^4$ to 4×10^4 M^{-1} s^{-1}. (d) Because dissociation of alcohol is followed by the rapid, quasi-irreversible reaction of the $E(NAD^+)$ complex with pyrazole, the rate of the reverse process (step k_{-e}) can be considered negligible. Therefore, the following rate and equilibrium constants and initial concentrations were used to calculate the time courses shown in Figure 6B: $k_b' = 2.5 \times 10^4$ M^{-1} s^{-1}; $k_{-b} = 2.5 \times 10^3\ s^{-1}$; $k_c = 500\ s^{-1}$; $k_{-c} = 1\ s^{-1}$; k_e

$= 2\ s^{-1}$; $k_{-c} = 0\ s^{-1}$; $k_g = 5 \times 10^3\ M^{-1}\ s^{-1}$; $K_a^S = 1\ \mu M$; $K = 1 \times 10^{-4}$ M; $[E(NADH)]_0 = 10\ \mu N$; $[HOnPhCHO]_0 = 100\ \mu M$; $[Pyr]_0 = 20$ mM; pH 8.75.

Random noise of ±2% has been introduced into the theoretical time courses to more realistically simulate the experimental data. The simulations were obtained by numerical integration of the differential rate expressions (via the Runge–Kutta method) for each of the species in Scheme I. Traces a, b, and c of Figure 6B compare the disappearance of substrate (a) and the disappearance of E(NADH) (b) with the appearance and decay of $E(NAD^+, HOnPhCH_2O^-)$ (c). The solid, noise-free curves drawn through the theoretical time courses are the computer-generated best fits of the theoretical data, assuming the time course consists of either two exponentials (trace c) with rate constants k_f and k_s or a single exponential (traces a and b). With the above assumptions, it is evident that the fit of each trace is adequate and that the rate constant for the slow phase (k_s) obtained from the biphasic fit of trace c is nearly identical with the best fit rate constants obtained for traces a and b. Only trace amounts of the ternary complex E(NADH, HOnPhCHO) were found to accumulate.

The rates k_f and k_s were found to be sensitive to changes in the concentration of $^-$OnPhCHO. When k_c of Scheme I is changed from 500 to 250 s^{-1} to simulate a primary isotope effect of $k_c^H/k_c^D = 2.0$, the rate of the slow phase is decreased such that $k_s^H \simeq 1.5$ (data not shown). Only at the very start of the reaction is the formation of intermediate uncomplicated by the appearance of product; Figure 6B illustrates the problem of determining the exact nature of the spectrum of E(X). Conversely, toward the end of the reaction there are still significant concentrations of reactants contributing to the absorbance changes.

It is clear from these simulations that when appropriate rate and equilibrium parameters are assigned to the individual steps shown in Scheme I, the mechanism reduces in complexity to a system of two apparent relaxations and that the dependencies of these two relaxations on substrate concentration, pH, and the substitution of NADD for NADH are fully consistent with the properties exhibited by the HOnPhCHO system.

Electrostatic Effects in LADH Catalysis. Scheme I proposes a structure for E(X) in which the phenolic hydroxyl is neutral, while the hydroxymethyl group is ionized to the alkoxide ion.

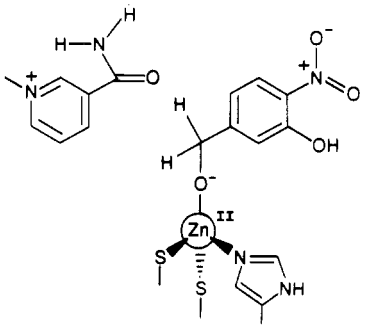

This structure implies that the pK_a of the phenolic hydroxyl is perturbed to a higher value by >2 pK_a units [i.e., we detect E(X) at pH >8.75] and the pK_a of the $-CH_2OH$ group is perturbed to a lower value by >7 pK_a units (from ~16 in aqueous solution to <9 in the ternary complex).

The blue shifting of the chromophore spectrum, as E(X) is formed, is consistent with a structure for E(X) in which the phenolic hydroxyl is neutral. While there is no direct evidence pertaining to the pK_a of the $-CH_2OH$ group within the E(X) intermediate, the work of Kvassman et al. (1981), of Cook and Cleland (1981), and of Sartorius et al. (1987) has provided experimental evidence that strongly supports a catalytic mechanism wherein catalysis of alcohol oxidation by LADH occurs via inner-sphere-coordinated alkoxide ion (the reactive species). According to the interpretation of Kvassman et al. (1981), within the ternary $E(NAD^+$, alcohol) complex, the apparent pK_a of inner-sphere-coordinated alcohol falls in the range 4.3–6.6 and depends upon the electronic structure of the substrate. The ternary complexes involving 2,2,2-trifluoroethanol, ethanol, and β-naphthaldehyde have been assigned pK_a values of 4.5, 6.4, and 6.6, respectively (Kvassman et al., 1981; Shore et al., 1974; Kvassman & Pettersson, 1980). If these pK_a assignments are correct, then it is reasonable to expect a pK_a for the inner-sphere-coordinated hydroxymethyl group of $HOnPhCH_2OH$ (eq 10) that is <9, and perhaps as low as 6 or 7.

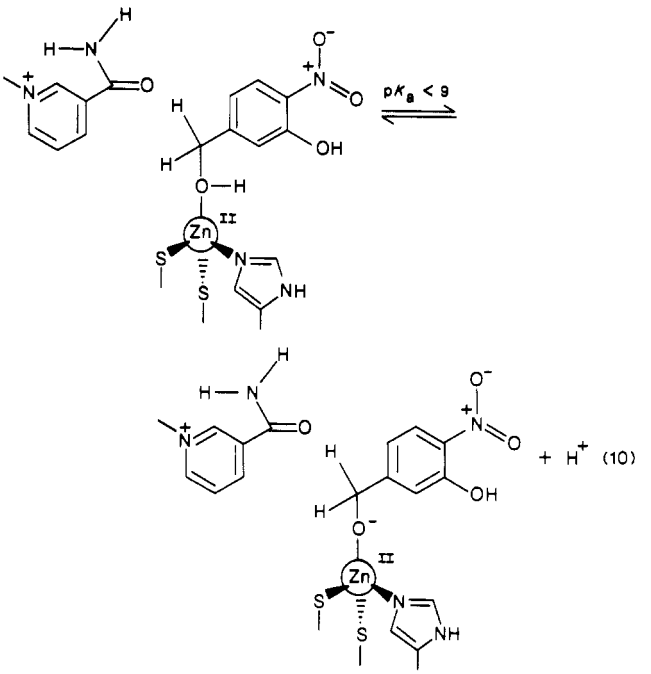

A combination of factors have been proposed to bring about these pK_a perturbations. Formation of an inner-sphere coordination complex with zinc ion is known to cause large perturbations in the pK_a for the coordinated ligand. For example, the aquated zinc ion has a pK_a of about 9.0 (Sillén & Martell, 1964, 1970), and Woolley (1975) has described a small molecule–pentacoordinate zinc complex containing a water molecule with $pK_a = 8.7$. The X-ray structures of LADH and various LADH binary and ternary complexes with small molecules and dinucleotides have been solved. These structures indicate that, in the absence of coenzyme, LADH almost always crystallizes in an orthorhombic space group, whereas most ternary complexes involving NADH and a small molecule (substate or analogue) coordinated to the active-site zinc ion crystallize in monoclinic or triclinic space groups (Brändén et al., 1975). The orthorhombic form is characterized by an "open" structure in which the active-site cavity is filled by a lattice of hydrogen-bonded water molecules (Ekland et al., 1976). The monoclinic and triclinic forms have undergone a conformational change to a "closed" structure in which the dimensions of the substrate binding cleft are reduced and, due to the reduced volume of the cleft and to the presence of substrate (or analogue), the lattice of water molecules is no longer present. These structural changes greatly alter the microenvironment of the site. The strength of the net electrostatic field emanating from the active-site zinc ion and from NAD^+ must be increased in the closed

structure *because* the lattice of water molecules (which, if present, would attenuate the effective electrostatic field via dielectric effects) is displaced. This increase in field strength further promotes formation of the alkoxide ion like species from the inner-sphere-coordinated alcohol. Since the alkoxide is most reasonably expected to be the species that undergoes oxidation via hydride transfer to NAD^+, decreasing the pK_a of coordinated alcohol increases the concentration of the reactive species and lowers the activation energy for hydride transfer. It then appears that the conformation change between open and closed forms makes possible a more polar catalytic site within the closed conformation via the exclusion of water, while conversion to the open form makes possible the facile exchange of coenzyme and substrate/product.

The X-ray structures of ternary complexes (Cedergren-Zeppezauer, 1982; Ekland et al., 1982) predict that the phenolic hydroxyl of coordinated $HOnPhCH_2OH$ should reside in a nonpolar region of the substrate binding cleft, thus accounting for the shift of the pK_a of the phenolic hydroxyl to a higher value. The perturbations of the pK_a values for the $-CH_2OH$ group and for the phenolic hydroxyl in opposite directions must reflect a steep gradient in the electrostatic field in the vicinity of the active site–binding site, such that the active site is more polar than water, while only a few angstroms away the binding cleft provides a hydrocarbon-like milieu. We conclude that it is the hydrocarbon-like environment of the substrate biding cleft that prevents the binding and reaction of $^-OhPhCHO$ and $^-OnPhCH_2OH$.

References

Abdallah, M. A., Biellman, J.-F., Cedergren-Zeppezauer, E., Gerber, M., Dietrich, H., Zeppezauer, M., Koerber, S. C., MacGibbon, A. K. H., & Dunn, M. F. (1984) *Biochemistry 23*, 1003–1015.

Andersson, P., Kvassman, J., Oldén, B., & Pettersson, G. (1981) *Eur. J. Biochem. 118*, 119–123.

Becker, N. H., & Roberts, J. D. (1984) *Biochemistry 23*, 3336–3340.

Bernasconi, C. F. (1976) in *Relaxation Kinetics*, pp 20–39, Academic, New York.

Bernhard, S. A., Dunn, M. F., Luisi, P. L., & Schack, P. (1970) *Biochemistry 9*, 185–192.

Brändén, C.-I., Jörnvall, H., Eklund, H., & Furugren, B. (1975) *Enzymes (3rd Ed.) 11*, 103–190.

Burr, M., & Koshland, D. E., Jr. (1964) *Proc. Natl. Acad. Sci. U.S.A. 52*, 1017–1024.

Cedergren-Zeppezauer, E., Samama, J.-P., & Eklund, H. (1982) *Biochemistry 21*, 4895–4908.

Conrad, R. H., Heitz, J. R., & Brand, L. (1970) *Biochemistry 9*, 1540–1546.

Cook, P. E., & Cleland, W. W. (1981) *Biochemistry 20*, 1805–1816.

Dahl, K. H., & Dunn, M. F. (1984a) *Biochemistry 23*, 4094–4100.

Dahl, K. H., & Dunn, M. F. (1984b) *Biochemistry 23*, 6829–6839.

Dunn, M. F. (1974) *Biochemistry 13*, 1146–1151.

Dunn, M. F. (1985) in *Enzymology of Carbonyl Metabolism 2: Aldehyde Dehydrogenase, Aldo-Keto Reductase and Alcohol Dehydrogenase* (Flynn, T. G., & Weiner, H., Eds.) pp 151–168, Liss, New York.

Dunn, M. F., & Hutchison, J. S. (1973) *Biochemistry 12*, 4882–4892.

Dunn, M. F., & Bernhard, S. A. (1974) *Tech. Chem. 8*, 619–691.

Dunn, M. F., Bernhard, S. A., Anderson, D., Copeland, A., Morris, R. G., & Rogue, J.-P. (1979) *Biochemistry 18*, 2346–2354.

Dunn, M. F., Dietrich, H., MacGibbon, A. K. H., Koerber, S. C., & Zeppezauer, M. (1982) *Biochemistry 21*, 354–363.

Dunn, M. F., MacGibbon, A. K. H., & Peace, K. (1986) in *Progress in Inorganic Biochemistry and Biophysics* (Bertini, I., Gray, H., & Zeppezauer, M., Eds.) pp 485–505, Birkhauser, Basel, Switzerland.

Eklund, H., Nördstrom, B., Zeppezauer, E., Söderlund, G., Ohlsson, I., Böiwe, T., Söderberg, B.-O., Tapia, O., Brändén, C.-I., & Åkeson, Å. (1976) *J. Mol. Biol. 102*, 27–59.

Eklund, H., Samana, J.-P., & Wallén, L. (1982) *Biochemistry 21*, 4858–4866.

Frey, P. A., Kokesh, F. C., & Westheimer, F. H. (1971) *J. Am. Chem. Soc. 93*, 7266–7269.

Frost, A. A., & Pearson, R. G. (1961) *Kinetics and Mechanisms*, pp 166–169, Wiley, New York.

Gerber, M., Zeppezauer, M., & Dunn, M. F. (1983) *Inorg. Chim. Acta 79*, 161–164.

Koerber, S. C., Schack, P., Au, A. M.-J., & Dunn, M. F. (1980) *Biochemistry 19*, 731–738.

Koerber, S. C., MacGibbon, A. K. H., Dietrich, H., Zeppezauer, M., & Dunn, M. F. (1983) *Biochemistry 22*, 3424–3431.

Kvassman, J., & Pettersson, G. (1978) *Eur. J. Biochem. 87*, 417–427.

Kvassman, J., & Pettersson, G. (1980) *Eur. J. Biochem. 103*, 565–575.

Kvassman, J., Larsson, A., & Pettersson, G. (1981) *Eur. J. Biochem. 114*, 555–563.

Laidler, K. J., & Bunting, P. S. (1973) in *The Chemical Kinetics of Enzyme Action*, pp 181–195, Clarendon Press, Oxford, England.

Luisi, P. L., & Bignetti, E. (1974) *J. Mol. Biol. 88*, 653–670.

McFarland, J. T., & Bernhard, S. A. (1972) *Biochemistry 11*, 1486–1493.

Morris, R. G., Saliman, G., & Dunn, M. F. (1980) *Biochemistry 19*, 725–731.

Sartorius, C., Gerber, M., Zeppezauer, M., & Dunn, M. F. (1987) *Biochemistry 26*, 871–882.

Shore, J. D., Gutfreund, H., Brooks, R. L., Santiago, D., & Santiago, P. (1974) *Biochemistry 13*, 4185–4191.

Sigman, D. S., & Glazer, A. N. (1972) *J. Biol. Chem. 247*, 334–341.

Sillén, L. G., & Martell, A. E. (1964) in *Stability Constants of Metal-Ion Complexes*, Part II, p 61, The Chemical Society, Burlington House, London.

Sillén, L. G., & Martell, A. E. (1970) in *Stability Constants of Metal-Ion Complexes*, Part III, p 27, The Chemical Society, Burlington House, London.

Woolley, P. (1975) *Nature (London) 258*, 677–682.